Published in final edited form as:

FASEB J. 2020 April ; 34(4): 4918–4933. doi:10.1096/fj.201902075R.

GORAB promotes embryonic lung maturation through antagonizing AKT phosphorylation, versican expression and mesenchymal cell migration

Ying Liu[1,6], **Xi Chen**[2,3,6], **Yeon Ja Choi**[2,§], **Ning Yang**[2], **Zhongya Song**[2,4], **Elizabeth R. Snedecor**[2], **Wei Liang**[1], **Elaine Lai-Han Leung**[3], **Lianfeng Zhang**[1], **Chuan Qin**[1,*], **Jiang Chen**[1,2,5,*]

[1]Institute of Laboratory Animal Science, Chinese Academy of Medical Science; and Comparative Medical Center, Peking Union Medical College; Key Laboratory of Human Disease Comparative Medicine, Ministry of Health, Beijing, China

[2]Department of Pathology, Stony Brook University, Stony Brook, NY 11794

[3]State Key Laboratory of Quality Research in Chinese Medicine, Macau University of Science and Technology, Macau, China

[4]Department of Dermatology, Peking University First Hospital, Beijing, China

[5]Department of Dermatology, Stony Brook University, Stony Brook, NY 11794

[6]These authors contributed equally to this work

Abstract

Embryonic development of the alveolar sac of the lung is dependent upon multiple signaling pathways to coordinate cell growth, migration, and the formation of the extracellular matrix. Here, we identify GORAB as a regulator of embryonic alveolar sac formation as genetically disrupting the *Gorab* gene in mice resulted in fatal saccular maturation defects characterized by a thickened lung mesenchyme. This abnormality is not associated with impairments in cellular proliferation and death but aberrantly increased AKT phosphorylation, elevated *Vcan* transcription, and enhanced migration of mesenchymal fibroblasts. Genetically augmenting PDGFRα, a potent activator of AKT in lung mesenchymal cells, recapitulated the alveolar phenotypes, whereas disrupting PDGFRα partially rescued alveolar phenotypes in *Gorab*-deficient mice. Overexpressing or suppressing *Vcan* in primary embryonic lung fibroblasts could respectively mimic or attenuate alveolar sac-like phenotypes in a co-culture model. These findings suggest a role of GORAB in negatively regulating AKT phosphorylation, the expression of *Vcan*, and the

[*]Correspondence: Jiang Chen, MD, Department of Pathology, Renaissance School of Medicine, Stony Brook University, Stony Brook, NY 11794, Phone: 631-444-3211, jiang.chen@stonybrook.edu, Chuan Qin, PhD, Institute of Laboratory Animal Science, Comparative Medical Center, Peking Union Medical College (PUMC), Chinese Academy of Medical Science (CAMS), Beijing, 100021, China, Phone: 0086-10-6777-0815, Fax: 0086-10-6771-0812, qinchuan@pumc.edu.cn.

[§]Current address: Department of Biopharmaceutical Engineering, College of Science and Technology, Dongguk University Gyeongju, Gyeongbuk, South Korea

AUTHOR CONTRIBUTIONS

Y. Liu, X. Chen, C. Qin, J. Chen designed research; Y. Liu, X. Chen, Y, Y.J. Choi, N. Yang, Z. Song, E. R. Snedecor, W. Liang, and J. Chen performed research; Y. Liu, E.L. Leung, L. Zhang, and C. Qin contributed new reagents and methods; Y. Liu, X. Chen, C. Qin, and J. Chen analyzed data; Y. Liu, X. Chen, C. Qin, J. Chen wrote the paper.

migration of lung mesenchyme fibroblasts, and suggest that alveolar sac formation resembles a patterning event that is orchestrated by molecular signaling and the extracellular matrix in the mesenchyme.

Keywords

morphogenesis; signaling; co-culture; VCAN; PDGF; fibroblast

INTRODUCTION

GORAB (golgin, RAB6-interacting), also known as SCYL1BP1 or NTKL-BP1, is a member of the coiled-coil proteins localized to the Golgi that are collectively called the golgins. The *GORAB* gene is widely expressed in tissues. Mutations in *GORAB* are associated with geroderma osteodysplasticum (1), characterized by premature aging of the bone and skin. GORAB physically interacts with RAB6 and ARF5 and is believed to function in intracellular trafficking (1, 2). GORAB is also implicated in bone and hair follicle formation (3, 4), neurite outgrowth (5), sciatic nerve regeneration (6), and tumor cell growth (7–9).

GORAB is expressed in the lung (1, 3, 6). We found that homozygous neonates of *Gorab* knockout (*Gorab*$^{-/-}$) mouse models exhibited severe breathing difficulties and fully penetrant neonatal lethality (3), suggesting that GORAB plays a critical role in the embryonic morphogenesis of the respiratory or the cardiovascular system.

The morphogenesis of the lung can be arbitrarily divided into five stages−embryonic, pseudoglandular, canalicular, saccular, and alveolar. The saccular stage is an intermediate stage when branching morphogenesis ceases and alveolarization is yet to start. In this stage, the terminal airways are growing in length and are widening, forming clusters of larger airspaces. The widening of the terminal airways is accompanied by condensation of the mesenchyme, the formation of primary septa, and the population of smooth muscle cell precursors that lay down a fibrous network comprised of elastic fibers and collagen fibrils (10).

In rodents, proper development of the saccular stage, the last stage prior to birth, directly correlates with the survival of neonates in which the lung starts to function as a gas exchange organ. Impaired saccular development, associated with thickened mesenchyme and reduced number of alveolar septum, almost always correlates with lethal perinatal respiratory distress (Supplemental References). The thickened mesenchyme is often correlated with increased cellular proliferation or decreased apoptosis during saccular maturation. Counter-intuitively, the massive thinning of the mesenchyme does not necessarily match with the limited rate of proliferation or apoptosis in the saccular lung (11, 12). Thus, potent drivers for mesenchymal thin-down or alveolar septum formation remains elusive.

Throughout the development and maturation of the lung, the epithelial and mesenchymal cells, primary resident cells of the lung, interact extensively through a complex network of

molecular signaling pathways, including fibroblast growth factor (FGF), bone morphogenetic protein (BMP), transforming growth factor (TGF)-β, wingless (Wnt), hedgehog, and platelet-derived growth factor (PDGF) (Reviewed in (13–16)). Deregulating these signaling pathways often results in lung morphogenesis abnormalities characterized by a thickened mesenchyme or poorly developed alveolar septa. In addition to regulating cellular proliferation, how these signaling pathways instruct the behavior or functions of the cells in the developing lung remains to be understood.

The PDGF signaling pathway is a potent stimulator of cell growth, differentiation, and motility of connective tissue cells. This signaling pathway is activated when PDGF ligands bind to PDGF receptors (PDGFRs), which dimerize and undergo autophosphorylation, thereby phosphorylating and activating AKT, one of the key downstream mediators of the PDGF signaling pathway (17). PDGF signaling is widely implicated in morphogenesis, tissue repair, pathogenesis of vascular and fibrotic diseases, and cancer (17, 18). Its role in lung morphogenesis and lung pathogenesis are extensively studied (reviewed in (19)).

During lung morphogenesis, the PDGF signaling pathway functions in a paracrine manner (20). The PDGF ligands, predominantly PDGF-AA (and also PDGF-C), are released by alveolar epithelial cells, whereas PDGF receptor alpha (PDGFRα) are expressed on mesenchymal cells and respond to ligand activation (20, 21). Disrupting the PDGF signaling pathway at the ligand or receptor level impairs lung mesenchymal maturation (22–28). Pertinent to this study, activating the PDGF signaling pathway through overexpressing PDGF-A (25), PDGF-C (29), or expressing hyperactive form of PDGFRα (26), consistently resulted in a thickened mesenchyme without affecting branching morphogenesis. However, downstream targets of the PDGF signaling pathway during lung morphogenesis remain to be characterized.

In this study, we discovered that GORAB is a critical regulator of lung alveolar sac formation. Disrupting the *Gorab* gene in mice led to the aberrant activation of AKT downstream of the PDGFR signaling pathway, increased transcription of versican (*Vcan*), and accelerated migration of lung mesenchymal fibroblasts. These findings substantiated the critical roles of the extracellular matrix and cellular migration during saccular maturation of the lung.

MATERIALS AND METHODS

Mouse models and tissue processing

Mice deficient of *Gorab* (*Gorab*$^{-/-}$) was described previously (3). The *Pdgfra-EGFP* (B6.129S4-*Pdgfra*$^{tm11(EGFP)Sor/J}$) mouse model was purchased from the Jackson Laboratory (Stock #007669, Bar Harbor, ME). The *Pdgfra/J* mouse model was a gift from the laboratory of Dr. Lorin Olson. The *Gorab* conditional knockout mouse model (*Gorab-flox* (4)) was a gift from the laboratory of Dr. Uwe Kornak. The *Twist2-cre* (B6.129X1-Twist2tm1.1(cre)Dor/J) mouse model was obtained from the Jackson Laboratory (Stock #008712). Wild-type (*Gorab*$^{+/+}$) littermates were used as controls. BrdU labeling was performed by intraperitoneal injection of 10 μl per gram of body weight of the BrdU labeling reagent (Thermo Fisher Scientific, Carlsbad, CA) two hours prior to euthanization.

All procedures relating to mice were performed in accordance with the Guide for the Care and Use of Laboratory Animals of the National Institutes of Health of the United States, and approved by the Institutional Animal Care and Use Committee of Stony Brook University (approval number 2012–1974-R2–9.14.18-MI).

Freshly isolated lungs were either imaged directly under a dissection microscope (Zeiss, Stemi 2000C), snap frozen in liquid nitrogen for RNA and protein extraction, or fixed in formalin and processed for embedding in paraffin, sectioning, and hematoxylin and eosin (H&E) staining or other examinations. For the floating test, lungs were collected from newborn pups and placed in 0.01 M PBS to determine buoyancy. Histological sections were examined on a Nikon 80i (Nikon, Melville, NY) microscope.

Cell culture and *in vitro* assays

The isolation of primary fibroblasts from mouse embryonic lung was performed as described (30, 31). Lungs were dissected from E18.5 embryos, minced with scissors, and incubated in 0.05% Trypsin-EDTA at 37°C for 15 minutes. The tissue lysate were then passed five times through a 22 G needle fitted on a syringe to dissociate cells. Cells were resuspended and plated in growth medium (Dulbecco's Modified Eagle Medium with 4.5g/L d-Glucose, L-Glutamine, 110mg/L Sodium Pyruvate (Gibco 11995–065, Thermo Fisher Scientific), supplemented with 10% FBS, and 100 μg/ml penicillin and streptomycin) in L-poly-lysine coated plates, and cultured overnight at 37°C in an incubator containing 5% CO_2. Growth medium was then replaced every other day until the cells reached 80% confluency.

Knockdown was performed by transfecting 15 nM siRNAs (siRNAs for mouse *Gorab*: 5'-UGAAUGAGACGCAUACAAAUUUAAA-3' or 5'-GCAGAAUAAAGAUCCAUUUGAACCT-3'; mouse *Vcan*: 5'-UCAUAUUUAUCAACAUCUUGUCCUU-3', 5'-CAUUUGAUUCUGAGAAAUUCACUCG-3', or 5'-UGUAGUCCUGACCAAUCUUGAUAUU-3') (IDT, Coralville, IA) with Lipofectamine RNAiMAX transfection reagent (Thermo Fisher Scientific, Waltham, MA) in medium containing 0.25% FBS per manufacturer's recommendations, and harvested or further manipulated 48 hours thereafter. Mouse *Vcan* cDNA (V2) was obtained from Origene (MR225930, Rockville, MD) and transfected (1 μg per well of 12-well plate) to mouse primary lung fibroblasts as described for siRNA.

Epithelial-mesenchymal co-culture

The epithelial-mesenchymal co-culture was performed as described (32). Primary lung mesenchymal cells or mouse embryonic fibroblasts were plated at high density (2×10^6/well of 6-well plate) the day before 2×10^6/well A549 cells (ATCC® CRM-CCL-185™) were added. Co-cultures were cultured in F-12K Medium (Gibco 21127–022) with 10% FBS and 100 μg/ml penicillin and streptomycin. Medium was replaced daily. The A549 cells were prestained with CellTracker™ Red CMPTX dyes (C34552, Thermo Fisher Scientific). Cells were fixed with 2% paraformaldehyde for 30 minutes at room temperature for analysis.

Quantifications of the lung and co-cultures

H&E sections were measured with the Image-Pro Plus 6.0 software (Media Cybernetics, Rockville, MD). For each group, at least 3 sections were imaged, and 6 randomly selected fields were measured per section. Quantitative assessment of the lung structure was performed per standards established by the American Thoracic Society/European Respiratory Society (33).

Co-cultured cells were fixed before phase-contrast images were taken by a Leica DMi 8 microscope and a Leica DFC9000 GT CCD camera (Leica, Wetzlar, Germany). Images were analyzed by Image-Pro Plus 6.0 to determine the thickness of ridges and area of pockets. The height of the ridges was determined in the z-plane from the top of the ridge to the monolayer of cells adjacent to the peak. For each independent experiment, at least 10 fields were imaged, and at least 3 ridges per field were measured.

To quantify immunofluorescence results, three randomly selected fields were imaged. The number of positive cells or structures (AQP5, proSFTPC, F-actin, VCAN, BrdU, TUNEL, bronchioles, or large blood vessels) were counted and were presented as a percentage of total cells (determined by nuclei stained with DAPI), or an average number of cells or structures per microscopic field. A minimum of three pairs of littermates obtained from different litters was evaluated throughout this study.

Cell migration assay

Primary fetal lung fibroblasts were plated in 6-well plates and cultured to 90% confluency. A scratch was introduced using a 200 μl pipette tip before the cells were washed with PBS and grown in serum-free media. The migration of cells into the scratched area was recorded for up to 24 hours using Leica DMi 8 microscope and a Leica DFC9000 GT CCD camera. For quantification, the wound gap was measured by using Image-Pro Plus 6.0, and normalized to that at 0 hours. Cell traces were measured by using the Olympus cellSens software (Olympus, Waltham, MA).

Flow cytometry

Cells were suspended in FACS buffer (2% FBS/DPBS), and incubated with respective antibodies. 7-Amino-Actinomycin D (7-AAD) (559925, BD Pharmingen, San Jose, CA) was used to gate live cells. To label cells, cells were incubated with antibodies for 30 minutes in the dark at 4°C, and then washed with D-PBS and pelleted by centrifugation at 1,500 RPM for 5 minutes. Cell pellets were resuspended in 2% paraformaldehyde, and analyzed by BD LSRFortessa cell analyzer (BD Biosciences, San Jose, CA). An average of 20,837 ± 9,403 cells were analyzed for controls, and 20,265 ± 7,222 cells were analyze for mutants per experiment. A minimum of three experiments were performed with lungs obtained from independent littermates. The following antibodies were used in flow cytometry: CD45-PE (130–102-781, Miltenyi Biotec, Somerville, MA), CD140a-BV421 (566293, BD Horizon, San Jose, CA); CD326-APC (563478, BD Pharmingen), CD31-FITC (561813, BD Pharmingen); alpha smooth muscle actin-FITC (ab8211, Abcam, Cambridge, MA).

RNA isolation and quantitative RT-PCR

RNA was isolated with RNeasy kit (Qiagen, Germantown, MD) and quantitative reverse-transcription polymerase chain reaction (qRT-PCR) analyses were performed. Complementary DNA was synthesized from 2 μg of total mRNA using a High Capacity cDNA Reverse Transcription kit (Thermo Fisher Scientific) and random hexameric primers. Real-time qRT-PCR was performed on ABI Prism 7500 (Thermo Fisher Scientific) with the following TaqMan probes: *Gorab*, Mm00724788_m1; *Aqp5*, Mm00437578_m1; *Sftpc*, Mm00488144_m1, *Vcan*, Mm01283063_m1; and glyceraldehyde-3-phosphate dehydrogenase (*Gapdh*), Mm99999915_g1 (Thermo Fisher Scientific). Results were analyzed using ΔΔCt method. Relative expression levels of target genes were determined by comparing with wild type or treatment controls after normalizing with *Gapdh*.

In situ hybridization

In situ hybridization was carried out on formalin-fixed paraffin embedded tissue sections using the RNAScope system (Advanced Cell Diagnostic, Hayward, CA) per manufacturer's instructions and as previously described (34, 35).

Western blotting

Protein was extracted from tissue or cell in cold radioimmunoprecipitation assay buffer (RIPA buffer) (50 mM Tris-HCl pH 7.4, 150 mM NaCl, 1% Triton X-100, 1% sodium deoxycholate, and 0.1% SDS) supplemented with proteinase/phosphotase inhibitors (Thermo Fisher Scientific). Tissue or cell lysates were cleared and separated by 10% SDS-PAGE and transferred to polyvinylidene fluoride (PVDF, Millipore, Burlington, MA) or Hybond nitrocellulose (GE Healthcare, Chicago, IL) membranes, following standard procedures. Blots were probed with primary antibodies which were then detected with HRP-conjugated secondary antibodies (BD biosciences, San Jose, CA) and SuperSignal substrates (Thermo Fisher Scientific). Enhanced chemiluminescent (ECL) substrate (Pierce, Rockford, IL USA) and CL-XPosure film (Thermo Fisher Scientific) were used for detection. The following primary antibodies were used: GORAB, 1:1,000 (Proteintech, Rosemont, IL); AQP5, 1:50 (A4979, MilliporeSigma, St. Louis, MO); SFTPC, 1:250 (ab40879, Abcam, Cambridge, MA); VCAN, 1:250 (AB1032, MilliporeSigma, Billerica, MA); p-AKT, 1:1,000 (S473, 4060s, CST, Beverly, MA); p-AKT, 1:1,000 (T308, 13038s, CST); AKT, 1:1,000 (9272s, CST); PDGF-AA, 1:500 (07–1436, MilliporeSigma); PHLPP2, 1:500 (ab71973, Abcam); PDGFRα, 1:500 (3174, CST); p-PDGFRα, 1:500 (Y1018, 4547, CST); GAPDH, 1:1,000 (ab9485, Abcam); β-actin (ACTB), 1:2,000 (SC-47778, Santa Cruz, Santa Cruz, CA). GAPDH and ACTB were used as loading controls. Quantification was performed with densitometry and ImageJ software (1.43u, National Institutes of Health, Bethesda, MD).

Immunofluorescence labeling, TUNEL, and microscopy

Immunofluorescence labeling of tissue specimens was performed by fixing tissue sections or cells in 4% PFA/PBS and blocking in 1% BSA (or permeated with 0.1% Triton X-100/PBS for 10 min for GORAB staining) prior to incubating with primary antibodies. The following primary antibodies were used: GORAB, 1:500 (Proteintech); AQP5, 1:50 (A4979, MilliporeSigma); SFTPC, 1:250 (ab40879, Abcam); VCAN, 1:200 (ab1032,

MilliporeSigma); VIM, 1:200 (ab92547, Abcam); F-actin, 1:50 (ab205, Abcam,); VCL, 1:100 (ab129002, Abcam); SCGB1A1, 1:200 (sc-365992, Santa Cruz); ACTA2, 1:500 (a2547, MilliporeSigma); CDH1, 1:100 (BD-610182, BD biosciences). AlexaFluor-conjugated secondary antibodies (1:250) were from Life Technologies (Thermo Fisher Scientific). Sections were sealed in mounting medium with DAPI (Vector Laboratories, Burlingame, CA). TUNEL staining was performed according to manufacturer's instructions (DeadEnd Fluoremetric, G3250, Promega, Chicago, IL). Images were acquired by Nikon 80i fitted with a Nikon DS-Qi1Mc camera and processed with Photoshop 5.5 CS (Adobe, San Jose, CA).

Statistical analyses

All quantifications are presented as means ± SD. Student *t*-test or Bonferroni's multiple comparison tests were used as indicated. One-way ANOVA was also conducted using the GraphPad software. $P < 0.05$ was considered statistically significant.

RESULTS

Gorab is essential for neonatal respiration and the development of alveolar sac

The *Gorab* gene is ubiquitously expressed in mouse embryonic lung, as demonstrated by *in situ* hybridization (Fig. 1A). In the previously reported *Gorab* null ($Gorab^{-/-}$) mouse models (3), the *Gorab* transcripts and the GORAB protein were essentially undetectable in the lungs of E18.5 $Gorab^{-/-}$ embryos (Fig. 1A–C).

All $Gorab^{-/-}$ neonates gasped for air, developed cyanosis, and died within minutes of birth (Fig. 1D and (3)), indicating the possibility of respiratory distress. Indeed, the lung of $Gorab^{-/-}$ neonates appeared under-inflated (Supplemental Fig. 1A and B). Wild-type ($Gorab^{+/+}$) and heterozygous ($Gorab^{+/-}$) littermates were indistinguishable. The lobulation of lungs biopsied from E18.5 $Gorab^{-/-}$ fetuses were normal (Supplemental Fig. 1D), but the edge of $Gorab^{-/-}$ lungs appeared denser (Fig. 1E, indicated by arrowheads), and the $Gorab^{-/-}$ lungs weigh less (45.6 ± 5.5 mg in control and 33.6 ± 6.2 mg in $Gorab^{-/-}$) (Supplemental Fig. 1E).

Hematoxylin and eosin (H&E) staining of neonatal and E18.5 embryonic lungs revealed a thickened mesenchyme at the expense of the alveolar sac space and septa in the $Gorab^{-/-}$ lung (Supplemental Fig. 1C and Fig. 1F). Lungs in E15.5 $Gorab^{-/-}$ embryos appeared indistinguishable from control littermates (Supplemental Fig. 1F), suggesting that disrupting *Gorab* does not affect canalicular but saccular development of the lung. Quantifications demonstrated that the alveolar sac area in the E18.5 $Gorab^{-/-}$ lungs was significantly reduced in comparison to control littermates (1606.65 ± 317.19 μm^2 in control and 648.29 ± 229.79 μm^2 in $Gorab^{-/-}$) (Fig. 1G). The alveolar sac chord length was also significantly reduced (31.88 ± 1.76 μm in control and 15.49 ± 1.70 μm in $Gorab^{-/-}$) (Fig. 1H), whereas the thickness of alveolar septa in $Gorab^{-/-}$ lung was significantly increased (9.05 ± 0.98 μm in control and 19.64 ± 1.69 μm in $Gorab^{-/-}$. n > 5 mice per group) (Fig. 1I). The numbers of bronchioles, marked by secretoglobin family 1A member 1 (SCGB1A1 or CC10), E-cadherin (CDH1), and alpha smooth muscle actin (α-SMA or ACTA2), were comparable in controls and $Gorab^{-/-}$ lungs (23.75 ± 2.06 and 17.00 ± 4.76, respectively). However, fewer

of bronchioles in the *Gorab*$^{-/-}$ lungs were to connect to the alveolar sacs (18.00 ± 2.45 in control and 11.50 ± 2.65 in *Gorab*$^{-/-}$) (Supplemental Fig. 2A–C), suggesting a defective in alveolar sac formation. In addition, large blood vessels were increased in *Gorab*$^{-/-}$ lungs (Supplemental Fig. 2D).

Cellular differentiation, proliferation and apoptosis are unimpaired in *Gorab*$^{-/-}$ lung

A number of prior studies attributed thickened lung mesenchyme to increased cellular proliferation, diminished apoptosis, or both. Here, BrdU labeling revealed comparable proliferating cells (3.39 ± 2.20% in control and 4.37 ± 1.56% in *Gorab*$^{-/-}$. n = 3 mice per group, $P = 0.56$) in the distal regions of the lungs (Fig. 1J and Supplemental Fig. 3A). TUNEL staining detected few albeit comparable number of apoptotic cells (0.26 ± 0.04% in control and 0.35 ± 0.12%. n = 3 mice per group, $P = 0.33$) in *Gorab*$^{-/-}$ fetuses (Fig. 1K and Supplemental Fig. 3B). These findings excluded the involvement of abnormal proliferation and cell death in the development of a thickened lung mesenchyme in *Gorab*$^{-/-}$ mutants.

Cellularity in the lungs of E18.5 fetuses were analyzed by flow cytometry. CD326-positive (CD326^{+}) epithelial cells (13.90 ± 4.22% in control and 13.65 ± 2.19% in *Gorab*$^{-/-}$), CD45-positive (CD45^{+}) lymphocytes (7.98 ± 2.15% in control and 7.36 ± 1.53% in *Gorab*$^{-/-}$), and CD31-positive (CD31^{+}) endothelial cells (0.045 ± 0.014% in control and 0.034 ± 0.023% in *Gorab*$^{-/-}$) were comparable (Fig. 1L and M). Among the remaining mesenchymal cells, CD140A-positive (CD140A^{+}) (7.39 ± 4.85% in control and 9.07 ± 2.80% in *Gorab*$^{-/-}$) and ACTA2-positive (ACTA2^{+}) (3.24 ± 1.56% in control and 3.74 ± 1.27% in *Gorab*$^{-/-}$) cells were also comparable (Fig. 1M and N). These data suggest that the abnormal lung morphology in *Gorab*$^{-/-}$ mutants was unlikely caused by abnormal cellular proliferation, differentiation, or death.

Type I and type II alveolar epithelial cells were evaluated in more detail. First, qRT-PCR and western blotting demonstrated comparable levels of aquaporin 5 (AQP5) and surfactant associated protein C (SFTPC or proSFTPC), expressed by type I and type II alveolar epithelial cells, respectively, in the lungs of E18.5 control and *Gorab*$^{-/-}$ mutants (Fig. 2A and B). Immunofluorescence labeling of AQP5 and SFTPC not only demonstrated comparable numbers of type I (21.10 ± 5.32% in control; 19.58 ± 4.59% in *Gorab*$^{-/-}$, $P = 0.7278$) and type II alveolar epithelial cells (15.71 ± 2.65% in control and 14.72 ± 1.17% in *Gorab*$^{-/-}$. $P = 0.5886$), but also revealed comparable distribution (Fig. 2C), excluding significant impairments in association with the disruption of the *Gorab* gene.

Gorab-deficient lung exhibits increased versican transcription

In the absence of apparent change in cellularity and defects in epithelial cells, we focused our study on the extracellular matrix. Versican (VCAN) is a major proteoglycan of the extracellular matrix secreted by mesenchymal fibroblasts in the alveolar compartment. VCAN has been correlated with alveolar septum formation in the lung (36, 37). It is also required for the formation of septum of the heart (38–40) and the secondary palate (41) through a process that is believed to be analogous to the formation of the lung septum. Thus, we evaluated the expression of *Vcan*. *In situ* hybridization (Fig. 2D) and immunofluorescence labeling (Fig. 2E) demonstrated markedly upregulated *Vcan*

transcription (*Vcan-V2*) and translation (VCAN-V2) in the lung of E18.5 *Gorab*$^{-/-}$ fetuses, consistent with qRT-PCR (Fig. 2F) and western blotting (Fig. 2G). These data not only demonstrated that *Gorab* suppresses *Vcan* transcription in embryonic lung, but also associated elevated *Vcan* with impaired alveolar sac formation.

Impaired alveolar sac formation in *Gorab*$^{-/-}$ mice is associated with abnormalities in mesenchymal fibroblasts

Because VCAN is expressed by the mesenchymal but not other cell types in the embryonic lung, we focused our investigation on mesenchymal cells. First, we confirmed that VCAN expression was indeed robustly upregulated in primary mesenchymal fibroblasts isolated from E18.5 *Gorab*$^{-/-}$ fetuses by western blotting (Fig. 2H). Secondly, disrupting *Gorab* in the mesenchymal cells in the *Gorab*$^{flox/flox}$;*Twist2-cre* mice exhibited histological abnormalities resembling those in *Gorab*$^{-/-}$ mice (Supplemental Fig. 4A). Subsequently, we used a previously described co-culture model (32) to verify whether mesenchymal cells are functionally responsible for impaired alveolar sac formation *in vitro* by co-culturing A549 lung epithelial cells with primary lung mesenchymal fibroblasts isolated from E18.5 control and *Gorab*$^{-/-}$ mutants. Control fibroblasts supported the development of alveolar-like structure but *Gorab*$^{-/-}$ fibroblasts lapsed (Fig. 3A). Quantifications demonstrated significantly increased thickness and reduced height of cell ridges (Fig. 3A and B) and diminished area of cell pockets (Fig. 3A and B) in *Gorab*$^{-/-}$ fibroblast co-cultures, reminiscent of what were observed *in vivo*.

The organization of A549 cells and fibroblasts were revealed by CMTPX CellTracker dye for A549 cells and vimentin (VIM) for fibroblasts. In control co-cultures, A549 cells and fibroblasts appeared to intercalate at cell ridges, whereas cell pockets were occupied predominantly by fibroblasts (Fig. 3C). In *Gorab*$^{-/-}$ co-cultures, fibroblasts occupied most of the surface area, and loosely associated A549 cells (Fig. 3C). Primary mouse embryonic fibroblasts (MEFs) were co-cultured with A549 cells in a control experiment, in which alveolar-like structures did not form (Supplemental Fig. 4B). These data demonstrated that primary lung mesenchymal fibroblasts are primed to interact with epithelial cells to form an alveolar sac-like structure, for which *Gorab* plays an indispensable role.

To test whether the expression *Vcan* is functionally involved in alveolar sac formation, we overexpressed *Vcan* in wild-type primary lung mesenchymal fibroblasts followed by co-culturing with A549 epithelial cells. Cells overexpressing *Vcan* increased the thickness of the ridges, and deceased the height of ridges and the area of cell pockets (Fig. 3D and E), similarly to *Gorab*$^{-/-}$ fibroblasts, suggesting that increasing *Vcan* is sufficient to cause alveolar sac abnormalities. In contrast, knocking down *Vcan* in *Gorab*$^{-/-}$ primary lung fibroblasts rescued respective abnormalities (Fig. 3F and G). Taken together, these data suggest that *Vcan* is functionally related to the formation of alveolar sac downstream of *Gorab*.

Gorab-deficient lung mesenchymal fibroblasts are migratory

Because that VCAN is expressed by mesenchymal cells, and is known to regulate cellular migration (42–45), we investigated the migration of mesenchymal cell, and found that

primary lung mesenchymal cell isolated from E18.5 *Gorab*$^{-/-}$ embryos exhibited elevated level of F-actin positive stress fibers (Fig. 4A). Specifically, confluent cultures had a markedly increased proportion of *Gorab*$^{-/-}$ fibroblasts that exhibit stress fibers compared to control cells (72.69 ± 12.19% and 15.45 ± 1.19%, respectively) (Fig. 4B).

In a scratch assay (Fig. 4C), *Gorab*$^{-/-}$ fibroblasts at the leading edge had more dynamic trajectories than controls cells when randomly selected cell tracks were superimposed from their origins (Fig. 4D). By 24 hours, *Gorab*$^{-/-}$ fibroblasts covered a larger cell-free area (57.2 ± 5.8% in *Gorab*$^{-/-}$ and 25.9 ± 4.2% in controls) (Fig. 4E) and traveled a longer distance (377.68 ± 99.13 μm in *Gorab*$^{-/-}$ and 186.64 ± 41.57 μm in controls) (Fig. 4F) than control cells. The velocity of *Gorab*$^{-/-}$ migrating cells was also higher than that of controls (16.42 ± 4.31 μm/h in *Gorab*$^{-/-}$ and 8.11 ± 1.81 μm/h in controls) (Fig. 4G).

Immunofluorescence labeling (Fig. 4H) indicated that most of the migrating *Gorab*$^{-/-}$ fibroblasts (91.94 ± 10.55%) had increased expression of F-actin at the cortex of lamellipodia, in contrast to a small proportion in control fibroblasts (28.08 ± 15.83%) (Fig. 4I). Vinculin (VCL), a focal adhesion molecule, was polarized to the opposing side of F-actin-positive lamellipodia (Fig. 4H). Taken together, the data demonstrated that disruption of *Gorab* in lung mesenchymal fibroblasts primed the cells to be more migratory.

Elevated AKT phosphorylation in *Gorab*$^{-/-}$ mesenchymal cells

Increased transcription of *Vcan* in *Gorab*-deficient cells suggests that GORAB regulates *Vcan* through signaling. The PDGF signaling is a strong candidate because it is one of the most potent inducers of *Vcan* transcription (46, 47). Indeed, AKT, an important mediator of the PDGF signaling pathway, was aberrantly activated as both p-AKT (S473) and p-AKT (T308) were markedly increased in the lungs of *Gorab*$^{-/-}$ mutants (Fig. 5A). Interestingly, the levels of PDGF ligand (PDGF-AA), PDGFRα, and p-PDGFRα (Y1018) were unchanged in the *Gorab*$^{-/-}$ lungs (Fig. 5A). PHLPP2, a phosphatase capable of dephosphorylating S473 in AKT, was also comparable in the control and *Gorab*$^{-/-}$ lungs (Fig. 5A). The data suggest that *Gorab* can negatively regulate AKT phosphorylation downstream of the ligand-induced activation of the PDGF signaling pathway.

To determine whether AKT was activated in mesenchymal cells, primary lung fibroblasts were isolated from E18.5 embryos for western blotting. Indeed, p-AKT (S473) was elevated in cells isolated from *Gorab*$^{-/-}$ mutants in comparison to the controls (Fig. 5B). This finding substantiated the detrimental role of aberrantly activated AKT in mesenchymal cells during alveolar sac formation in the *Gorab*$^{-/-}$ lung and provided evidence supporting the role of AKT activity in promoting mesenchymal cell migration during morphogenesis (reviewed in (48)).

GORAB controls AKT phosphorylation downstream of PDGF pathway activation

To determine whether the elevated p-AKT in *Gorab*$^{-/-}$ mesenchymal fibroblasts was under the control of PDGF signaling, primary lung mesenchymal fibroblasts were treated with PDGF ligand (PDGF-AA). As expected, control cells expressed a low level of p-AKT (S473), whereas PDGF-AA was able to induce a robust upregulation of p-AKT (Fig. 5C, two left lanes). Strikingly, PDGF-AA was able to further increase the already elevated level

of p-AKT (S473) in *Gorab*$^{-/-}$ primary lung mesenchymal cells (Fig. 6C, two right lanes), suggesting that GORAB functions as an endogenous negative regulator of AKT phosphorylation, operating downstream yet independent of ligand-induced PDGF pathway activation.

Data obtained so far also suggest that aberrantly activating PDGF signaling, hence p-AKT, may result in alveolar sac formation defects, as seen in *Gorab*$^{-/-}$ mutants, and these abnormalities may be associated with elevated *Vcan* expression. To test this idea, we examined *Pdgfra/J* (26), a mouse model with an elevated basal PDGFRα kinase activity associated with the expression of an activating mutant PDGFRα (V561D) found in gastrointestinal stromal tumors. Heterozygous *Pdgfra/J* mice (*Pdgfra*$^{+/J}$) were able to survive to E18.5, and their lungs indeed exhibited slightly thickened mesenchyme (Fig. 5D). Although the thickened mesenchyme in *Pdgfra*$^{+/J}$ was not as remarkable as other PDGF pathway-activating mouse models (25, 26, 29), the alveolar sac area (1716.4 ± 338.1 μm^2 in control and 1267.2 ± 186.5 μm^2 in *Pdgfra*$^{+/J}$) and alveolar sac chord were significantly reduced in *Pdgfra*$^{+/J}$ mutants (36.4 ± 3.1 μm^2 in control and 26.8 ± 4.0 μm^2 in *Pdgfra*$^{+/J}$), whereas thickness of alveolar sac septum of *Pdgfra*$^{+/J}$ mutants was markedly increased (11.3 ± 0.8 μm in control and 17.4 ± 2.8 μm in *Pdgfra*$^{+/J}$) (Fig. 5E), partially phenocopied *Gorab*$^{-/-}$ mutants. Western blotting demonstrated increased p-AKT (S473) and elevated VCAN levels in the lungs of *Pdgfra*$^{+/J}$ mutants (Fig. 5F). These findings further substantiated the detrimental effect of increased AKT activation and VCAN during the maturation of the lung mesenchyme.

Suppressing AKT through PDGF signaling partially rescued lung phenotypes in *Gorab*$^{-/-}$ mutants

Considering that genetically activating the PDGF signaling pathway could result in lung phenotypes resembling that of *Gorab*$^{-/-}$ mutants (25, 26, 29) and that the data generated herein suggests that GORAB restrains AKT activation downstream of the PDGF signaling pathway, it is conceivable that suppressing the PDGF signaling pathways may attenuate elevated AKT phosphorylation in the developing lung of *Gorab*$^{-/-}$ mice. To test this hypothesis, we performed an *in vivo* rescue experiment by crossing *Gorab*$^{-/-}$ mutants with a loss-of-function allele of *Pdgfra* (*Pdgfra-EGFP*, (49)). The lungs of *Pdgfra*$^{+/EGFP}$ fetuses contained approximately half the amount of PDGFRα (CD140A) and EGFP-positive cells than *Gorab*$^{+/+}$;*PDGFRα*$^{+/+}$ littermates (Supplemental Fig. 5), and a diminished level of p-AKT (S473) (Fig. 6C), confirming PDGF signaling pathway suppression. *Gorab*$^{-/-}$ mutants that expressed one allele of PDGFRα-EGFP (*Gorab*$^{-/-}$;*Pdgfra*$^{+/EGFP}$) were able to survive to E18.5, and appeared indistinguishable from *Gorab*$^{-/-}$ (*Gorab*$^{-/-}$;*Pdgfra*$^{+/+}$) mutants, suggesting that the allele of *PDGFRα-EGFP* did not have a significant impact on the development of *Gorab*$^{-/-}$ embryos. However, at histological level, the lung of *Gorab*$^{-/-}$;*Pdgfra*$^{+/EGFP}$ fetuses exhibited an improved morphology in comparison to *Gorab*$^{-/-}$ (*Gorab*$^{-/-}$;*Pdgfra*$^{+/+}$) mutants (Fig. 6A). Specifically, the area of alveolar sac was significantly increased (1135.1 ± 153.4 μm^2 in *Gorab*$^{-/-}$;*Pdgfra*$^{+/EGFP}$ and 564.9 ± 34.9 μm^2 in *Gorab*$^{-/-}$;*Pdgfra*$^{+/+}$, n ≥ 3 mice per group, $P = 0.017$), alveolar chord length was significantly increased (25.6 ± 2.3 μm in *Gorab*$^{-/-}$;*Pdgfra*$^{+/EGFP}$ and 16.5 ± 1.3 μm in *Gorab*$^{-/-}$;*Pdgfra*$^{+/+}$,n ≥ 3 mice per group, $P < 0.008$), and the thickness of alveolar septa in *Gorab*

Gorab$^{-/-}$;*PDGFRα*$^{+/EGFP}$ mutants was significantly reduced (17.5 ± 1.9 μm in *Gorab*$^{-/-}$;*Pdgfrα*$^{+/EGFP}$ and 25.2 ± 1.5 μm in *Gorab*$^{-/-}$;*Pdgfrα*$^{+/+}$, n ≥ 3 mice per group, $P = 0.00002$) (Fig. 6B). These data demonstrated that attenuating AKT activation through suppressing PDGF signaling was effective in rescuing defects in alveolar sac formation in *Gorab*$^{-/-}$ mutants. The phenotypic improvement in *Gorab*$^{-/-}$;*PDGFRα*$^{+/EGFP}$ mutants was associated with a reduced level of VCAN as demonstrated by western blotting (Fig. 6C), *in situ* hybridization (Fig. 6D), and immunofluorescence labeling (Fig. 6E). These data suggest that increased AKT activation is one of the main drivers for the alveolar sac formation abnormalities in the *Gorab*$^{-/-}$ mutants, and VCAN is likely an important effector downstream of activated AKT.

In summary, data obtained from this study suggested that GORAB is a critical regulator of embryonic alveolar sac maturation by acting as an endogenous negative regulator of AKT phosphorylation downstream of the PDGF signaling pathway and that *Vcan* is an important downstream effector of AKT to organize the saccular region of the lung during the final stage of embryonic lung development.

DISCUSSION

The critical roles of the mesenchyme during lung morphogenesis, from respiratory specification, branching morphogenesis, and vascular development to alveolar maturation, is becoming increasingly evident (50). PDGF, one of the most extensively studied signaling pathways, plays prominent instructive roles on the lung mesenchyme cells during alveolarization (24). In this study, we demonstrated that increased p-AKT, a critical mediator of PDGF signaling, in *Gorab*$^{-/-}$ mutants contributed to increased expression of VCAN by the lung mesenchymal fibroblasts, a correlation also documented in vascular smooth muscle cells (51, 52). These findings underscore the importance of the PDGF-AKT-VCAN regulatory axis and suggest that the *Vcan* gene is an important transcriptional target during the maturation of the lung mesenchyme.

Premature aging of the bone and skin are the main manifestations of geroderma osteodysplasticum patients. Emphysema and frequent lung infection were reported in geroderma osteodysplasticum patients (53) but the incidence is too low to determine whether these respiratory symptoms are associated with this disease. Mutations in the *GORAB* gene have not yet been clearly associated with any lung disorder. Findings from the current study nevertheless suggest that disease-causing mutations, most of which are loss-of-function mutations, in the *GORAB* gene may impair the proper formation of alveoli during morphogenesis, thereby, subject patients to respiratory manifestations. Considering that disrupting *Gorab* in mice significantly increased AKT phosphorylation, whereas p-AKT is a potent inducer of extracellular matrix (collagen) production and is associated with fibrosis (54–56), it is conceivable that loss-of-function mutations in the *GORAB* may eventually result in fibrotic disorders in the lung and other organs.

The reduced alveolar sac formation and thickened mesenchyme seen in the lungs of *Gorab*$^{-/-}$ mutants are not associated with apparent impairments in cellular differentiation, proliferation, or apoptosis. Instead, data suggest that these phenotypes may be a result of defects in the extracellular matrix, the formation of which is deemed a prerequisite for

alveolarization (10). Thus, the composition of the extracellular matrix and mesenchymal cell migration should be evaluated when a thickened lung mesenchyme is encountered in order to deepen our understanding of the embryonic maturation of the lung.

VCAN is highly expressed in the perialveolar mesenchyme (57, 58). It is not only implicated in the formation of the alveolar septum in the embryonic and postnatal lung (36, 37), but also the formation of the cardiac septum (38–40) and the secondary palate of the oral cavity (41), suggesting that these analogous developmental events may be controlled by similar molecular and cellular mechanisms.

As the major type of proteoglycans in the extracellular matrix, VCAN is known to play a broad range of functions from signaling to the regulation of cellular proliferation, adhesion, and migration (42–45). Prior studies demonstrated that increased VCAN negatively correlates with the migration of primary lung fibroblasts obtained from lung-transplanted patients (59) and neural crest cells (60–63), probably through forming an exclusive boundary or acting as a guiding cue (62). In the current study, we found that primary mesenchymal fibroblasts that expressed an elevated level of VCAN were more migratory. These findings underscore the important functions of VCAN in cell migration which ought to be evaluated in a cell-, tissue-, and developmental stage-dependent manner.

VCAN has four splice variants (V0, V1, V2, and V3). The current study focused on VCAN-V2, which is expressed at a moderate level in the embryonic lungs in mice. Other variants (V0, V1, and V3) are also expressed in the embryonic lung (58). Whether these isoforms are similarly regulated by GORAB or perform similar functions during lung morphogenesis, remain to be further dissected. Recently, Chan et al. demonstrated that the expressions of decorin and biglycan, small proteoglycans, are also affected in *Gorab*-deficient mutant mice in the context of bone formation (4). Collectively, these findings suggest that GORAB plays a broad role in the formation of the extracellular matrices of connective tissues.

PDGF is one of the best understood signaling pathways capable of transcriptionally regulating *Vcan* in mesenchymal fibroblasts (46, 47). In the lung, PDGF-A, PDGF-C, and PDGFRα are predominant components of the PDGF signaling pathway and appear to have a prominent role in alveolar formation (20, 23, 24). In fact, PDGFRα signaling has already been implicated in mesenchymal cell migration during septum formation (64). Findings from the current study reinforced AKT as a critical effector of the activated PDGF signaling pathway to coordinate cellular migration during alveolar sac formation.

The identification of GORAB as an endogenous negative regulator of the PDGF signaling pathway in lung mesenchymal cells was unsuspected. Data suggest that GORAB regulates AKT downstream of PDGF receptor activation. Understanding the precise molecular mechanism through which GORAB inhibits AKT phosphorylation is beyond the scope of the current study. However, considering that AKT is a critical signaling node downstream a number of receptor tyrosine kinases (RTK) or G-protein–coupled receptors (GPCRs), uncovering GORAB as an endogenous negative regulator of AKT activation has important implications in embryonic morphogenesis, fibrosis, and tumor formation, in which these signaling mechanisms play critical roles.

Supplementary Material

Refer to Web version on PubMed Central for supplementary material.

ACKNOWLEDGEMENTS

We would like to thank Dr. Lorin Olson for sharing the *Pdgfra/J* mouse models, Dr. Uwe Kornak for sharing the *Gorab* conditional knockout mouse models, and the flow cytometry core facility of Stony Brook University for support. Zhongya Song was supported by the China Scholarship Council (No. 201706010325). This work was supported by CAMS initiative for Innovative Medicine (2016-12M-2-006), Macao Science and Technology Development Fund (Project No: 0096/2018/A3), and research grants from the Natural Science Foundation of China (31301928, 81472899, and 81773308) and the National Institute of Health of the United States of America (AR061485 and AR071573). The funders had no role in study design, data collection, data analysis, decision to publish, and preparation of the manuscript.

NONSTANDARD ABBREVIATIONS:

GORAB	Golgin, RAB6 Interacting
RAB6A	RAB6A, member RAS oncogene family
ARF5	ADP ribosylation factor 5
PDGF	platelet-derived growth factor
PDGFRα	PDGF receptor alpha
p-PDGFRα	phosphorylated PDGFRα
VCAN	versican
Sftpc	Surfactant Protein C
AQP5	aquaporin 5
AKT	protein kinase B
PHLPP2	PH aomain and leucine rich repeat protein phosphatase 2
CDH1	e-cadherin
EGFP	enhanced green fluorescent protein
GAPDH	glyceraldehyde-3-phosphate dehydrogenase
VCL	vinculin
VIM	vimentin
SCGB1A1	secretoglobin family 1A member 1, ACTA2, smooth muscle actin alpha 2
ACTB	β-actin
BSA	bovine serum albumin
BrdU	Bromodeoxyuridine/5-bromo-2’-deoxyuridine

EDTA	ethylenediaminotetraacetic acid
FITC	fluorescein isothiocyanate
H&E	hematoxylin and eosin
DAPI	4’ 6-diamidino-2-phenylindole
PFA	paraformaldehyde
PBS	phosphate buffered saline
FBS	fetal bovine serum
SDS	sodium dodecyl sulfate
PVDF	polyvinylidene fluoride
ECL	enhanced chemiluminescent
RNA	ribonucleic acid
siRNA	small interfering RNA
RTK	receptor tyrosine kinase
ECM	extracellular matrix
MEFs	mouse embryonic fibroblasts
PCR	polymerase chain reaction
qRT-PCR	quantitative reverse-transcription polymerase chain reaction
TUNEL	terminal deoxynucleotidyl transferase dUTP nick end labeling
RIPA	radioimmunoprecipitation assay
PAGE	polyacrylamide gel electrophoresis
FACS	fluorescence-activated cell sorting
P	postnatal day
E	embryonic day
M	molar
G	gauge

REFERENCES

1. Hennies HC, Kornak U, Zhang H, Egerer J, Zhang X, Seifert W, Kuhnisch J, Budde B, Natebus M, Brancati F, Wilcox WR, Muller D, Kaplan PB, Rajab A, Zampino G, Fodale V, Dallapiccola B, Newman W, Metcalfe K, Clayton-Smith J, Tassabehji M, Steinmann B, Barr FA, Nurnberg P, Wieacker P, and Mundlos S (2008) Gerodermia osteodysplastica is caused by mutations in SCYL1BP1, a Rab-6 interacting golgin. Nat. Genet. 40, 1410–1412 [PubMed: 18997784]

2. Egerer J, Emmerich D, Fischer-Zirnsak B, Chan WL, Meierhofer D, Tuysuz B, Marschner K, Sauer S, Barr FA, Mundlos S, and Kornak U (2015) GORAB Missense Mutations Disrupt RAB6 and ARF5 Binding and Golgi Targeting. J. Invest. Dermatol. 135, 2368–2376 [PubMed: 26000619]

3. Liu Y, Snedecor EL, Choi YJ, Ning Y, Zhang X, Xu Y, Han Y, Jones EC, Shroyer KR, Clark RA, Zhang L, Qin C, and Chen J (2016) Gorab is essential for dermal condensate cells to respond to hedgehog signals during hair follicle morphogenesis. J. Invest. Dermatol. 136, 378–386 [PubMed: 26967474]

4. Chan WL, Steiner M, Witkos T, Egerer J, Busse B, Mizumoto S, Pestka JM, Zhang H, Hausser I, Khayal LA, Ott CE, Kolanczyk M, Willie B, Schinke T, Paganini C, Rossi A, Sugahara K, Amling M, Knaus P, Chan D, Lowe M, Mundlos S, and Kornak U (2018) Impaired proteoglycan glycosylation, elevated TGF-beta signaling, and abnormal osteoblast differentiation as the basis for bone fragility in a mouse model for gerodermia osteodysplastica. PLoS Genet. 14, e1007242 [PubMed: 29561836]

5. Liu Y, Chen Y, Lu X, Wang Y, Duan Y, Cheng C, and Shen A (2012) SCYL1BP1 modulates neurite outgrowth and regeneration by regulating the Mdm2/p53 pathway. Mol. Biol. Cell 23, 4506–4514 [PubMed: 23051735]

6. Zhang W, Liu Y, Zhu X, Cao Y, Liu Y, Mao X, Yang H, Zhou Z, Wang Y, and Shen A (2016) SCY1-Like 1-Binding Protein 1 (SCYL1BP1) Suppressed Sciatic Nerve Regeneration by Enhancing the RhoA Pathway. Mol. Neurobiol. 53, 6342–6354 [PubMed: 26572638]

7. Yang ZP, Xie YH, Ling DY, Li JR, Jiang J, Fan YH, Zheng JL, and Wu WX (2014) SCYL1BP1 has tumor-suppressive functions in human lung squamous carcinoma cells by regulating degradation of MDM2. Asian Pac. J. Cancer Prev. 15, 7467–7471 [PubMed: 25227860]

8. Hu L, Liu M, Chen L, Chan TH, Wang J, Huo KK, Zheng BJ, Xie D, and Guan XY (2012) SCYL1 binding protein 1 promotes the ubiquitin-dependent degradation of Pirh2 and has tumor-suppressive function in the development of hepatocellular carcinoma. Carcinogenesis 33, 1581–1588 [PubMed: 22570270]

9. Yan J, Zhang D, Di Y, Shi H, Rao H, and Huo K (2010) A newly identified Pirh2 substrate SCYL1-BP1 can bind to MDM2 and accelerate MDM2 self-ubiquitination. FEBS lett. 584, 3275–3278 [PubMed: 20598683]

10. Schittny JC (2017) Development of the lung. Cell Tissue Res. 367, 427–444 [PubMed: 28144783]

11. Kresch MJ, Christian C, Wu F, and Hussain N (1998) Ontogeny of apoptosis during lung development. Pediatr. Res. 43, 426–431 [PubMed: 9505285]

12. Scavo LM, Ertsey R, Chapin CJ, Allen L, and Kitterman JA (1998) Apoptosis in the development of rat and human fetal lungs. Am. J. Respir. Cell Mol. Biol. 18, 21–31 [PubMed: 9448042]

13. Maeda Y, Dave V, and Whitsett JA (2007) Transcriptional control of lung morphogenesis. Physiol. Rev. 87, 219–244 [PubMed: 17237346]

14. Volckaert T, and De Langhe SP (2015) Wnt and FGF mediated epithelial-mesenchymal crosstalk during lung development. Dev. Dyn. 244, 342–366 [PubMed: 25470458]

15. Chao CM, El Agha E, Tiozzo C, Minoo P, and Bellusci S (2015) A breath of fresh air on the mesenchyme: impact of impaired mesenchymal development on the pathogenesis of bronchopulmonary dysplasia. Front. Med. (Lausanne) 2, 27 [PubMed: 25973420]

16. Kugler MC, Joyner AL, Loomis CA, and Munger JS (2015) Sonic hedgehog signaling in the lung. From development to disease. Am. J. Respir. Cell Mol. Biol. 52, 1–13 [PubMed: 25068457]

17. Andrae J, Gallini R, and Betsholtz C (2008) Role of platelet-derived growth factors in physiology and medicine. Genes Dev. 22, 1276–1312 [PubMed: 18483217]

18. Hoch RV, and Soriano P (2003) Roles of PDGF in animal development. Development 130, 4769–4784 [PubMed: 12952899]

19. Noskovicova N, Petrek M, Eickelberg O, and Heinzelmann K (2015) Platelet-derived growth factor signaling in the lung. From lung development and disease to clinical studies. Am. J. Respir. Cell Mol. Biol. 52, 263–284 [PubMed: 25303647]

20. Gouveia L, Betsholtz C, and Andrae J (2017) Expression analysis of platelet-derived growth factor receptor alpha and its ligands in the developing mouse lung. Physiol. Rep. 5, e13092 [PubMed: 28330949]

21. McGowan SE, Grossmann RE, Kimani PW, and Holmes AJ (2008) Platelet-derived growth factor receptor-alpha-expressing cells localize to the alveolar entry ring and have characteristics of myofibroblasts during pulmonary alveolar septal formation. Anat. Rec. 291, 1649–1661
22. Lindahl P, Karlsson L, Hellstrom M, Gebre-Medhin S, Willetts K, Heath JK, and Betsholtz C (1997) Alveogenesis failure in PDGF-A-deficient mice is coupled to lack of distal spreading of alveolar smooth muscle cell progenitors during lung development. Development 124, 3943–3953 [PubMed: 9374392]
23. Bostrom H, Gritli-Linde A, and Betsholtz C (2002) PDGF-A/PDGF alpha-receptor signaling is required for lung growth and the formation of alveoli but not for early lung branching morphogenesis. Dev. Dyn. 223, 155–162 [PubMed: 11803579]
24. Bostrom H, Willetts K, Pekny M, Leveen P, Lindahl P, Hedstrand H, Pekna M, Hellstrom M, Gebre-Medhin S, Schalling M, Nilsson M, Kurland S, Tornell J, Heath JK, and Betsholtz C (1996) PDGF-A signaling is a critical event in lung alveolar myofibroblast development and alveogenesis. Cell 85, 863–873 [PubMed: 8681381]
25. Li J, and Hoyle GW (2001) Overexpression of PDGF-A in the lung epithelium of transgenic mice produces a lethal phenotype associated with hyperplasia of mesenchymal cells. Dev Biol. 239, 338–349 [PubMed: 11784039]
26. Olson LE, and Soriano P (2009) Increased PDGFRalpha activation disrupts connective tissue development and drives systemic fibrosis. Dev. Cell 16, 303–313 [PubMed: 19217431]
27. Sun T, Jayatilake D, Afink GB, Ataliotis P, Nister M, Richardson WD, and Smith HK (2000) A human YAC transgene rescues craniofacial and neural tube development in PDGFRalpha knockout mice and uncovers a role for PDGFRalpha in prenatal lung growth. Development 127, 4519–4529 [PubMed: 11023856]
28. Gouveia L, Betsholtz C, and Andrae J (2018) PDGF-A signaling is required for secondary alveolar septation and controls epithelial proliferation in the developing lung. Development 145
29. Zhuo Y, Hoyle GW, Shan B, Levy DR, and Lasky JA (2006) Over-expression of PDGF-C using a lung specific promoter results in abnormal lung development. Transgenic Res. 15, 543–555 [PubMed: 16830225]
30. Benjamin JT, Gaston DC, Halloran BA, Schnapp LM, Zent R, and Prince LS (2009) The role of integrin alpha8beta1 in fetal lung morphogenesis and injury. Dev. Biol. 335, 407–417 [PubMed: 19769957]
31. Dieperink HI, Blackwell TS, and Prince LS (2006) Hyperoxia and apoptosis in developing mouse lung mesenchyme. Pediatr. Res. 59, 185–190 [PubMed: 16439576]
32. Greer RM, Miller JD, Okoh VO, Halloran BA, and Prince LS (2014) Epithelial-mesenchymal co-culture model for studying alveolar morphogenesis. Organogenesis 10, 340–349 [PubMed: 25482312]
33. Hsia CC, Hyde DM, Ochs M, and Weibel ER (2010) An official research policy statement of the American Thoracic Society/European Respiratory Society: standards for quantitative assessment of lung structure. Am. J. Respir. Crit. Care Med. 181, 394–418 [PubMed: 20130146]
34. Wang F, Flanagan J, Su N, Wang LC, Bui S, Nielson A, Wu X, Vo HT, Ma XJ, and Luo Y (2012) RNAscope: a novel in situ RNA analysis platform for formalin-fixed, paraffin-embedded tissues. J. Mol. Diagn. 14, 22–29 [PubMed: 22166544]
35. Chen J, Laclef C, Moncayo A, Snedecor ER, Yang N, Li L, Takemaru K, Paus R, Schneider-Maunoury S, and Clark RA (2015) The ciliopathy gene Rpgrip1l is essential for hair follicle development. J. Invest. Dermatol. 135, 701–709 [PubMed: 25398052]
36. Kugler MC, Loomis CA, Zhao Z, Cushman JC, Liu L, and Munger JS (2017) Sonic Hedgehog Signaling Regulates Myofibroblast Function during Alveolar Septum Formation in Murine Postnatal Lung. Am. J. Respir. Cell Mol. Biol. 57, 280–293 [PubMed: 28379718]
37. Bird AD, Choo YL, Hooper SB, McDougall AR, and Cole TJ (2014) Mesenchymal glucocorticoid receptor regulates the development of multiple cell layers of the mouse lung. Am. J. Respir. Cell Mol. Biol. 50, 419–428 [PubMed: 24053134]
38. Henderson DJ, and Copp AJ (1998) Versican expression is associated with chamber specification, septation, and valvulogenesis in the developing mouse heart. Circ. Res. 83, 523–532 [PubMed: 9734475]

39. Kruithof BP, Krawitz SA, and Gaussin V (2007) Atrioventricular valve development during late embryonic and postnatal stages involves condensation and extracellular matrix remodeling. Dev. Biol. 302, 208–217 [PubMed: 17054936]
40. Hatano S, Kimata K, Hiraiwa N, Kusakabe M, Isogai Z, Adachi E, Shinomura T, and Watanabe H (2012) Versican/PG-M is essential for ventricular septal formation subsequent to cardiac atrioventricular cushion development. Glycobiology 22, 1268–1277 [PubMed: 22692047]
41. Vaziri Sani F, Kaartinen V, El Shahawy M, Linde A, and Gritli-Linde A (2010) Developmental changes in cellular and extracellular structural macromolecules in the secondary palate and in the nasal cavity of the mouse. Eur. J. Oral Sci. 118, 221–236 [PubMed: 20572855]
42. Kinsella MG, Bressler SL, and Wight TN (2004) The regulated synthesis of versican, decorin, and biglycan: extracellular matrix proteoglycans that influence cellular phenotype. Crit. Rev. Eukaryot. Gene Expr. 14, 203–234 [PubMed: 15248816]
43. Rahmani M, Wong BW, Ang L, Cheung CC, Carthy JM, Walinski H, and McManus BM (2006) Versican: signaling to transcriptional control pathways. Can. J. Physiol. Pharmacol. 84, 77–92 [PubMed: 16845893]
44. Wight TN (2002) Versican: a versatile extracellular matrix proteoglycan in cell biology. Curr. Opin. Cell Biol. 14, 617–623 [PubMed: 12231358]
45. Theocharis AD (2008) Versican in health and disease. Connect. Tissue Res. 49, 230–234 [PubMed: 18661349]
46. Tiedemann K, Malmstrom A, and Westergren-Thorsson G (1997) Cytokine regulation of proteoglycan production in fibroblasts: separate and synergistic effects. Matrix Biol. 15, 469–478 [PubMed: 9106158]
47. Andersson-Sjoland A, Hallgren O, Rolandsson S, Weitoft M, Tykesson E, Larsson-Callerfelt AK, Rydell-Tormanen K, Bjermer L, Malmstrom A, Karlsson JC, and Westergren-Thorsson G (2015) Versican in inflammation and tissue remodeling: the impact on lung disorders. Glycobiology 25, 243–251 [PubMed: 25371494]
48. Xue G, and Hemmings BA (2013) PKB/Akt-dependent regulation of cell motility. J. Natl. Cancer Inst. 105, 393–404 [PubMed: 23355761]
49. Hamilton TG, Klinghoffer RA, Corrin PD, and Soriano P (2003) Evolutionary divergence of platelet-derived growth factor alpha receptor signaling mechanisms. Mol. Cell Biol. 23, 4013–4025 [PubMed: 12748302]
50. McCulley D, Wienhold M, and Sun X (2015) The pulmonary mesenchyme directs lung development. Curr. Opin. Genet. Dev. 32, 98–105 [PubMed: 25796078]
51. Osman N, Getachew R, Thach L, Wang H, Su X, Zheng W, and Little PJ (2014) Platelet-derived growth factor-stimulated versican synthesis but not glycosaminoglycan elongation in vascular smooth muscle is mediated via Akt phosphorylation. Cell. Sig. 26, 912–916
52. Evanko SP, Johnson PY, Braun KR, Underhill CB, Dudhia J, and Wight TN (2001) Platelet-derived growth factor stimulates the formation of versican-hyaluronan aggregates and pericellular matrix expansion in arterial smooth muscle cells. Arch. Biochem. Biophys. 394, 29–38 [PubMed: 11566024]
53. Rajab A, Kornak U, Budde BS, Hoffmann K, Jaeken J, Nurnberg P, and Mundlos S (2008) Geroderma osteodysplasticum hereditaria and wrinkly skin syndrome in 22 patients from Oman. Am. J. Med. Genet. A. 146A, 965–976 [PubMed: 18348262]
54. Hsu HS, Liu CC, Lin JH, Hsu TW, Hsu JW, Su K, and Hung SC (2017) Involvement of ER stress, PI3K/AKT activation, and lung fibroblast proliferation in bleomycin-induced pulmonary fibrosis. Sci. Rep. 7, 14272 [PubMed: 29079731]
55. Saito S, Zhuang Y, Shan B, Danchuk S, Luo F, Korfei M, Guenther A, and Lasky JA (2017) Tubastatin ameliorates pulmonary fibrosis by targeting the TGFbeta-PI3K-Akt pathway. PLoS One 12, e0186615 [PubMed: 29045477]
56. Zhang Y, and Stefanovic B (2016) Akt mediated phosphorylation of LARP6; critical step in biosynthesis of type I collagen. Sci. Rep. 6, 22597 [PubMed: 26932461]
57. Faggian J, Fosang AJ, Zieba M, Wallace MJ, and Hooper SB (2007) Changes in versican and chondroitin sulfate proteoglycans during structural development of the lung. Am. J. Physiol. Regul. Integr. Comp. Physiol. 293, R784–792 [PubMed: 17522116]

58. Snyder JM, Washington IM, Birkland T, Chang MY, and Frevert CW (2015) Correlation of Versican Expression, Accumulation, and Degradation during Embryonic Development by Quantitative Immunohistochemistry. J. Histochem. Cytochem. 63, 952–967 [PubMed: 26385570]

59. Andersson-Sjoland A, Thiman L, Nihlberg K, Hallgren O, Rolandsson S, Skog I, Mared L, Hansson L, Eriksson L, Bjermer L, and Westergren-Thorsson G (2011) Fibroblast phenotypes and their activity are changed in the wound healing process after lung transplantation. J. Heart Lung Transplant. 30, 945–954 [PubMed: 21624839]

60. Landolt RM, Vaughan L, Winterhalter KH, and Zimmermann DR (1995) Versican is selectively expressed in embryonic tissues that act as barriers to neural crest cell migration and axon outgrowth. Development 121, 2303–2312 [PubMed: 7671797]

61. Snow HE, Riccio LM, Mjaatvedt CH, Hoffman S, and Capehart AA (2005) Versican expression during skeletal/joint morphogenesis and patterning of muscle and nerve in the embryonic mouse limb. Anat. Rec. A. Discov. Mol. Cell. Evol. Biol. 282, 95–105 [PubMed: 15633171]

62. Szabo A, Melchionda M, Nastasi G, Woods ML, Campo S, Perris R, and Mayor R (2016) In vivo confinement promotes collective migration of neural crest cells. J. Cell Biol. 213, 543–555 [PubMed: 27241911]

63. Dutt S, Matasci M, Sommer L, and Zimmermann DR (2006) Guidance of neural crest cell migration: the inhibitory function of the chondroitin sulfate proteoglycan, versican. ScientificWorldJournal 6, 1114–1117 [PubMed: 16964367]

64. McGowan SE, and McCoy DM (2013) Platelet-derived growth factor-A and sonic hedgehog signaling direct lung fibroblast precursors during alveolar septal formation. Am. J. Physiol. Lung Cell Mol. Physiol. 305, L229–239 [PubMed: 23748534]

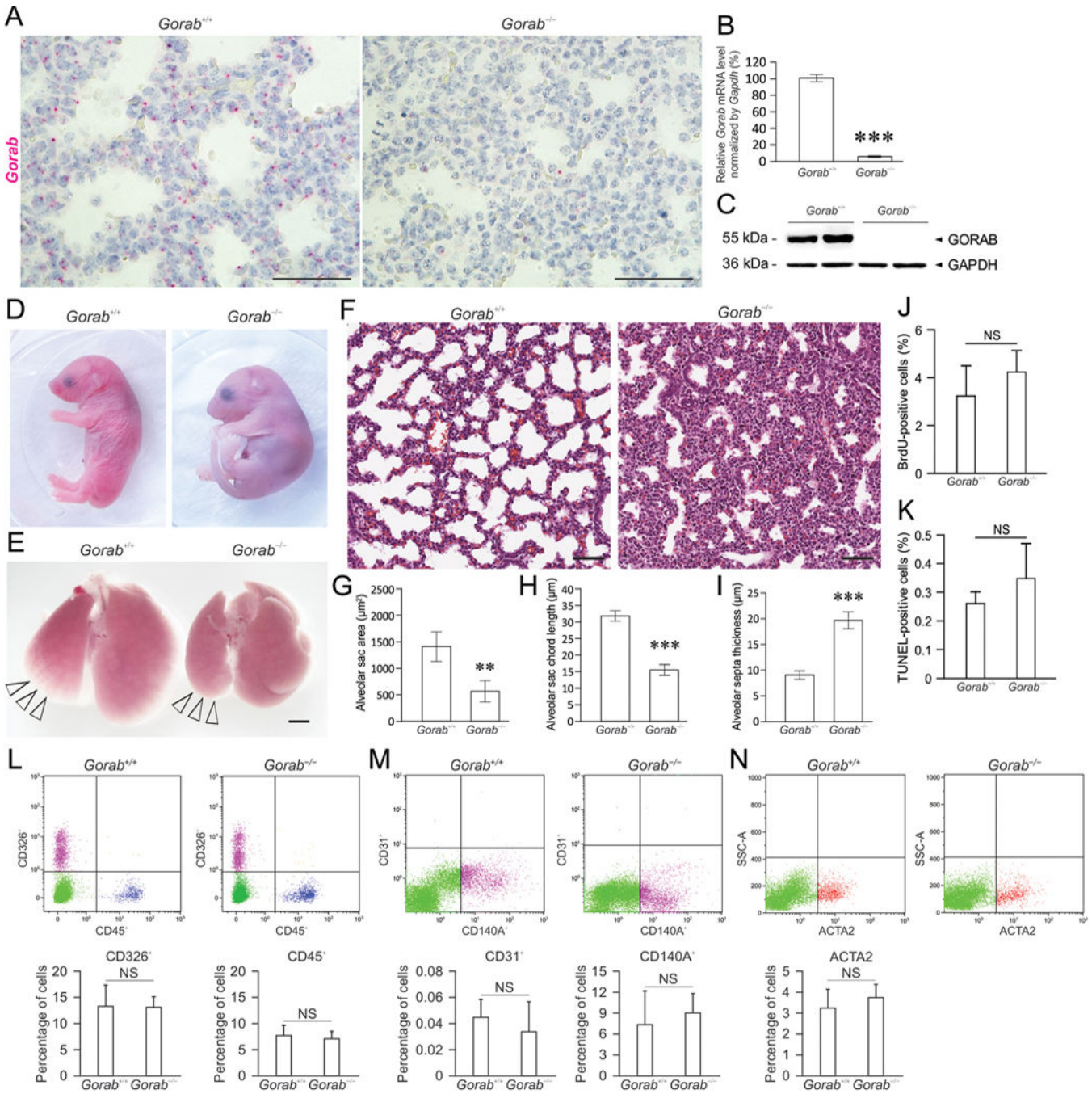

Figure 1. *Gorab* is involved in alveolar sac formation.

(**A - C**) Expression of *Gorab* in the lung of E18.5 wild-type (*Gorab*$^{+/+}$) or homozygous *Gorab* knockout (*Gorab*$^{-/-}$) mouse models by *in situ* hybridization (A, pink dots), qRT-PCR (B), and western blotting (C). (**D**) Appearance of newborn littermates, showing cyanosis in a *Gorab*$^{-/-}$ pup. (**E**) Gross appearance of the lungs dissected from E18.5 *Gorab*$^{+/+}$ or *Gorab*$^{-/-}$ fetuses. Arrows point to edges of the lung. (**F**) Hematoxylin and eosin staining of the distal regions of E18.5 lungs. (**G - I**) Quantifications of the areas of alveolar sacs (G), the length of alveolar sac chord (h), and the thickness of alveolar septum (I) (n ≥ 5/group). (**J**, **K**)

Quantification of BrdU-positive (J) or TUNEL-positive (K) cells in E18.5 *Gorab*$^{+/+}$ and *Gorab*$^{-/-}$ lung. n > 300 cells per three paired littermates. (**L - N**) Flow cytometry analysis (upper panels) and quantification (lower panels) of CD326-positive (CD326^{+}) epithelial cell (L), CD45-positive (CD45^{+}) leukocytes (L), CD31-positive (CD31^{+}) endothelial cells (M), CD140A-positive (CD140A^{+}) mesenchymal cells (M), alpha smooth muscle actin (ACTA2)-positive mesenchymal cells (N) isolated from E18.5 *Gorab*$^{+/+}$ and *Gorab*$^{-/-}$ lungs. 12,689 and 12,757 cells were analyzed for *Gorab*$^{+/+}$ and *Gorab*$^{-/-}$ lungs in (L), 17,762 and 15,938 cells were analyzed for *Gorab*$^{+/+}$ and *Gorab*$^{-/-}$ lungs in (M), and 10,453 and 9,402 cells were analyzed for *Gorab*$^{+/+}$ and *Gorab*$^{-/-}$ lungs in (N). SSC, side-scatter. Data are shown as means ± SD (n ≥ 3 pairs of littermates). ** $P < 0.01$, *** $P < 0.001$, NS, not statistically significant *vs*. corresponding controls. Scale bars, 50 μm (A, F), 1 mm (E).

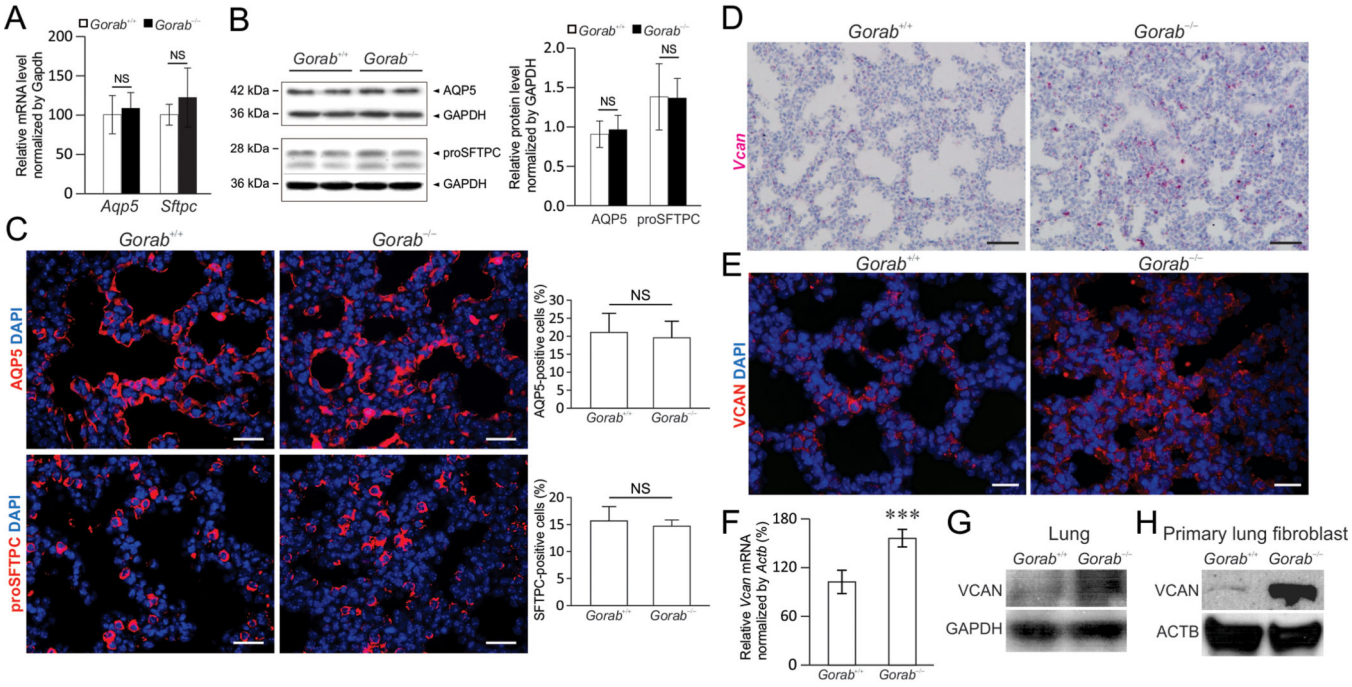

Figure 2. Evaluation of gene expression of epithelial and mesenchymal cells in E18.5 lungs.

(**A**, **B**) Quantification of type I (aquaporin 5, Aqp5) and type II (prosurfactant associated protein C, proSFTPC) epithelial markers by quantitative RT-PCR (a) and western blotting (B) in control (*Gorab*$^{+/+}$) and homozygous *Gorab* knockout mouse models (*Gorab*$^{-/-}$). (**C**) Immunofluorescence labeling of AQP5 and proSFTPC in lung of *Gorab*$^{+/+}$ or *Gorab*$^{-/-}$ fetuses, and quantification (n > 300 cells per three pairs of littermates). Nuclei are stained with DAPI (blue). (**D** - **G**) Evaluation of versican (*Vcan*) expression in the lung of control (*Gorab*$^{+/+}$) and homozygous *Gorab* knockout mouse models (*Gorab*$^{-/-}$) by *in situ* hybridization (D), immunofluorescence (E), quantitative RT-PCR (F), and western blotting (G). (**H**) Western blotting of VCAN in primary fibroblasts isolated from E18.5 *Gorab*$^{+/+}$ and *Gorab*$^{-/-}$ fetuses. Data are shown as means ± SD (n ≥ 3 pairs of littermates). ∗∗∗ $P < 0.001$, NS, not statistically significant *vs.* corresponding controls. Scale bars, 25 μm (C, E), 50 μm (D).

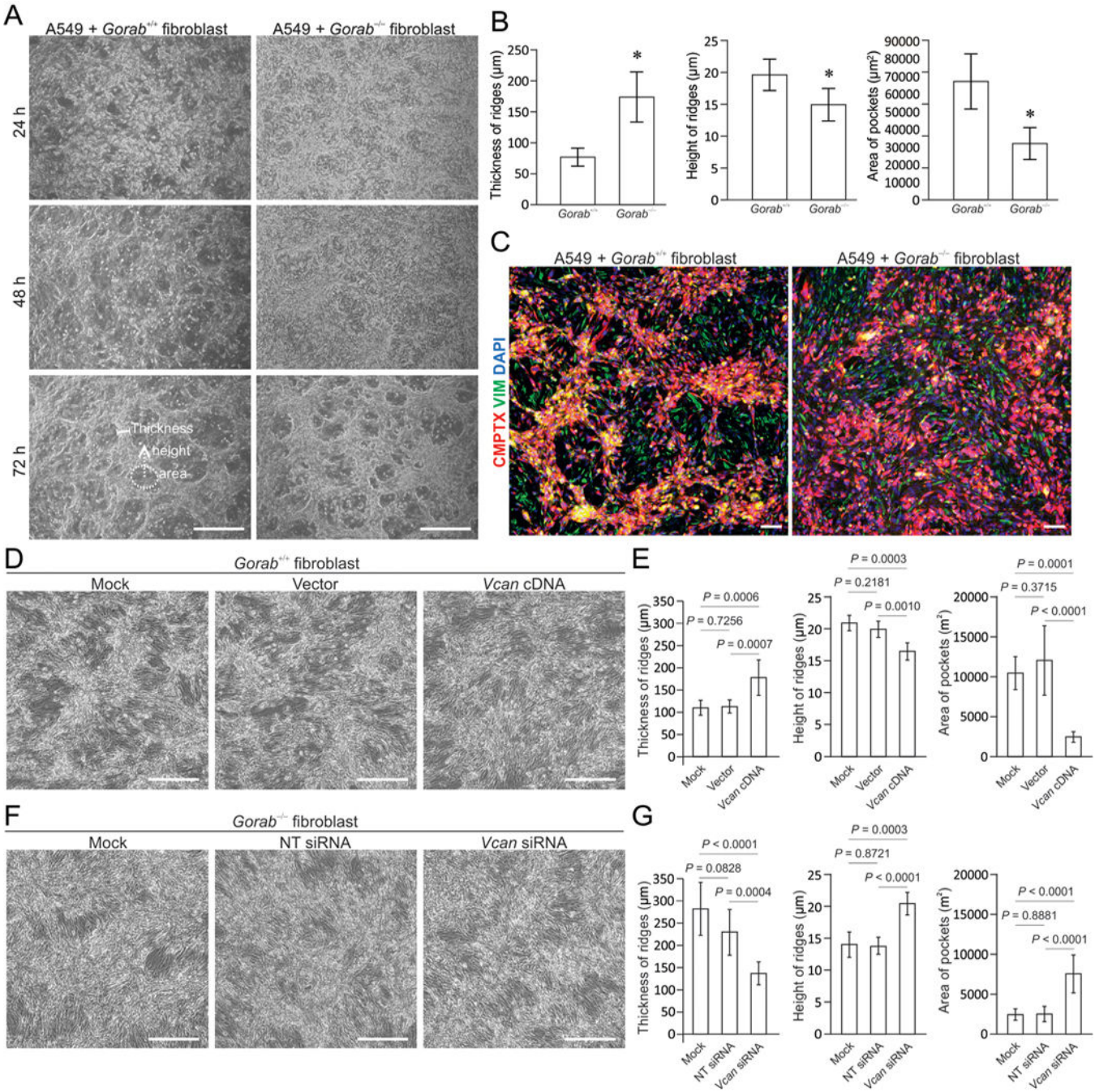

Figure 3. Co-culture of A549 epithelial cells with *Gorab*$^{-/-}$ mesenchymal cells.

(**A**) Appearance of alveolar-like structure formed by co-culturing A549 epithelial cells with primary fibroblasts isolated from lungs of E18.5 *Gorab*$^{+/+}$ or *Gorab*$^{-/-}$ fetuses for indicated durations. (**B**) Quantifications of the thickness (left) and height (middle) of cell ridge and the area of pockets (right) at 72 hours of co-culturing. (**C**) Representative distribution of cells in 72-hour co-cultures by immunofluorescence labeling of A549 (CellTracker dye CMTPX, red) and fibroblasts (vimentin, VIM, green). (**D - E**) Appearance (D) and quantification (E) of alveolar-like structure formed by co-culturing A549 epithelial cells with primary

fibroblasts isolated from the lungs of wild type E18.5 *Gorab*$^{+/+}$ fetuses and transfected with *Vcan-V2* cDNA or Vector. Mock indicates non-transfected cells. Cells were examined 48 hours after transfection. (**F - G**) Appearance (F) and quantification (G) of alveolar-like structure formed by co-culturing A549 epithelial cells with primary fibroblasts isolated from the lungs of E18.5 *Gorab*$^{-/-}$ fetuses and transfected with *Vcan* siRNA or non-targeting (NT) siRNA. Mock indicates non-transfected cells. Cells were examined 48 hours after transfection. Data are shown as means ± SD (n ≥ 3 independent experiments). Student's *t*-test and Bonferroni's multiple comparison test, one-way ANOVA. ∗ $P < 0.05$ *vs.* corresponding controls. Scale bars, 500 μm (A), 100 μm (C), 250 μm (D, F).

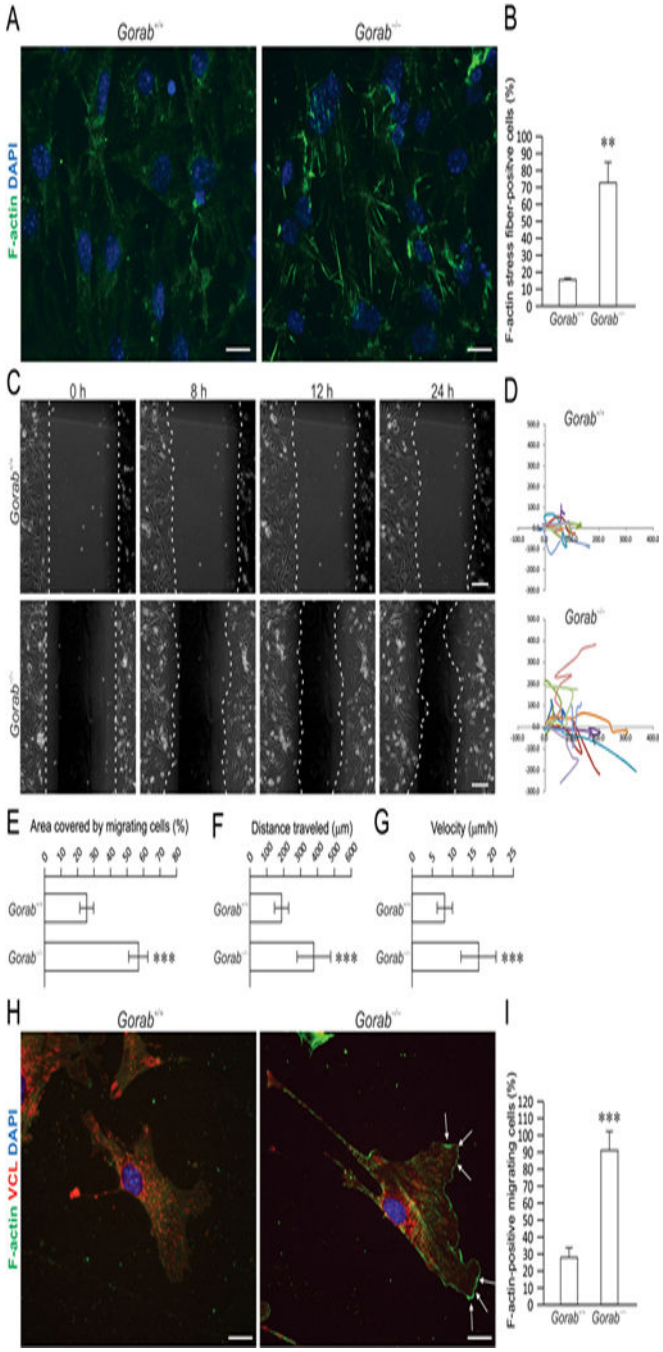

Figure 4. Migratory phenotypes of *Gorab*$^{-/-}$ mesenchymal cells.

(**A**) Immunofluorescence labeling of F-actin (green) in quiescent primary lung mesenchymal cells isolated from the lung of E18.5 *Gorab*$^{+/+}$ or *Gorab*$^{-/-}$ fetuses. (**B**) Quantification of F-actin-positive stress fibers. (**C**) Phase-contrast image of *Gorab*$^{+/+}$ or *Gorab*$^{-/-}$ primary lung mesenchymal cells in scratch assay. Dotted lines outline the cell borders. n > 100 cells per experiment. (**D**) Super-imposed migration tracks of 10 randomly selected cells at the border over 24 hours. (**E - G**) Quantification of scratched areas covered by migrating cell (E), and the distance and velocity of migrating cells. n = 30 randomly selected cells per three

independent experiments. (**H**) Representative immunofluorescence images of F-actin (green) and vinculin (VCL, red) in cells migrating into the scratched area. Arrows indicate F-actin-positive lamellipodia. (**I**) F-actin-positive cells at border or within the scratched area. n = 30. Data are shown as means ± SD (n = 3 independent experiments). ∗∗ $P < 0.01$, ∗∗∗ $P = 0.001$ *vs.* corresponding controls. Scale bars, 20 μm (A, H), 200 μm (C).

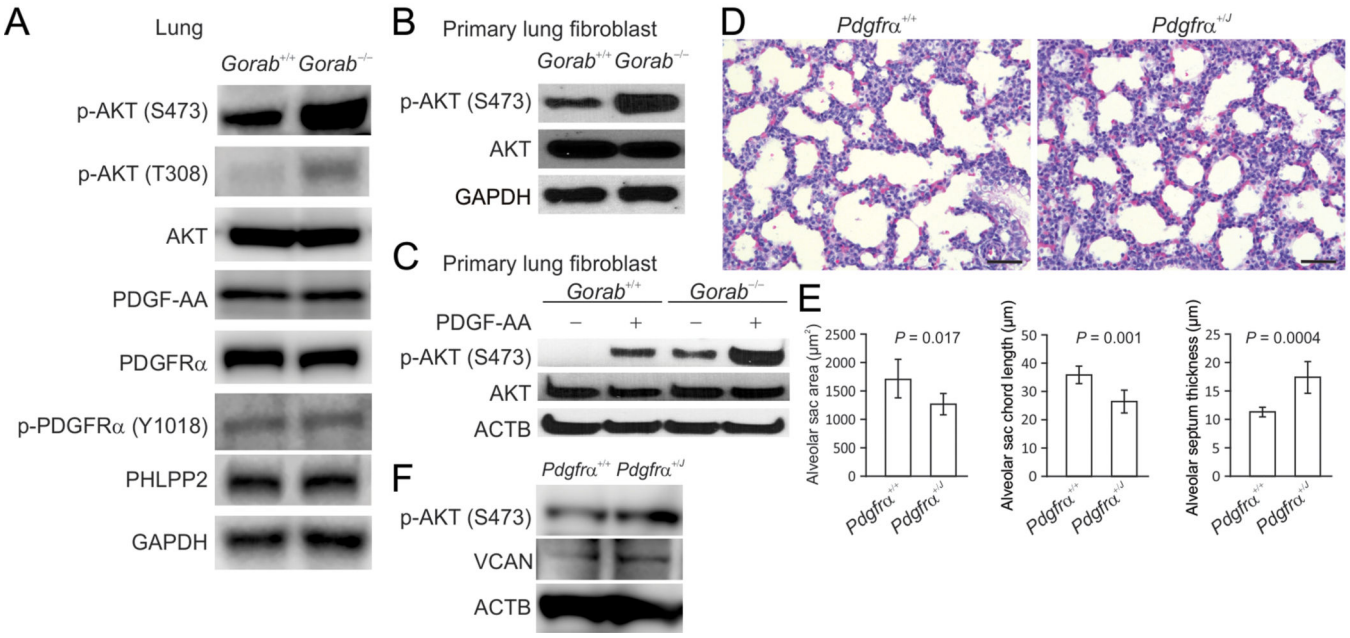

Figure 5. AKT activity in the lung.

(**A**) Western blotting of phospho-AKT (p-AKT S473 and S308), PDGF signaling components, and PHLPP2 in the lung of E18.5 control (*Gorab*$^{+/+}$) and homozygous *Gorab* knockout mouse models (*Gorab*$^{-/-}$). (**B**) Western blotting of p-AKT in primary fibroblasts isolated from the lung of E18.5 *Gorab*$^{+/+}$ and *Gorab*$^{-/-}$ fetuses (n ≥ 3 pairs of littermates). (**C**) Western blotting of p-AKT in primary mesenchymal cells treated with PDGF-AA. (**D**) H&E staining of distal regions of the lungs biopsied from E18.5 wild type (*Pdgfrα*$^{+/+}$) and heterozygous *Pdgfrα*$^{+/J}$ mutants. (**E**) Quantifications of the area of alveolar sac (left), the length of alveolar sac chord (middle), and the thickness of alveolar septum (right). (**F**) Western blotting of p-AKT and VCAN in the lung of E18.5 *Pdgfrα*$^{+/+}$ and *Pdgfrα*$^{+/J}$ mutants. All experiments were performed with a minimum of 3 pairs of littermates. Data are shown as means ± SD (n = 3 mice/group). Scale bars, 50 μm.

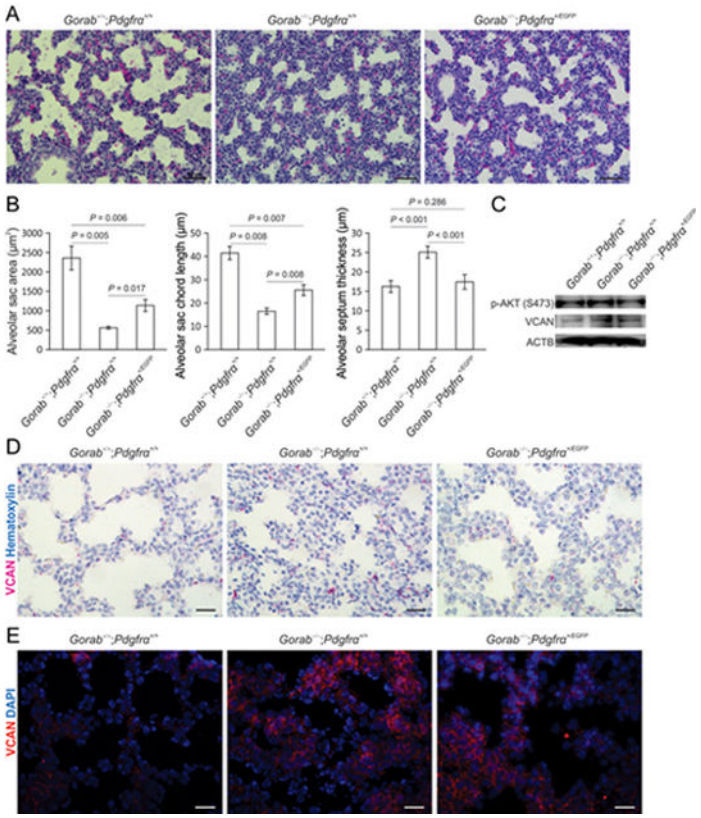

Figure 6. Attenuating PDGF/AKT ameliorating lung phenotypes in *Gorab*$^{-/-}$ mutants.

(**A**) H&E staining of distal regions of the lungs of wild type (*Gorab*$^{+/+}$;*PDGFRα*$^{+/+}$), homozygous *Gorab* mutant (*Gorab*$^{-/-}$;*PDGFRα*$^{+/+}$), and homozygous *Gorab* mutant deficient for PDGF receptor α (*Gorab*$^{-/-}$;*PDGFRα*$^{+/EGFP}$). (**B**) Quantifications of the area of alveolar sac (left), the length of alveolar sac chord (middle), and the thickness of alveolar septum (right) (n = 3 pairs of littermates). (**C**) Western blotting of p-AKT and VCAN in lungs described in (A). (**D**, **E**) *In situ* hybridization (D) and immunofluorescence labeling (E) of VCAN in lungs described in (A). Nuclei are stained with hematoxylin (D) or DAPI (E). All experiments were performed with a minimum of 3 pairs of littermates. Data are shown as means ± SD (n = 3 mice/group). Bonferroni's multiple comparison test, one-way ANOVA. Scale bars, 50 μm (A), 25 μm (D, E).